Proceedings of the ASME 2018
Dynamic Systems and Control Conference
DSCC2018
September 30-October 3, 2018, Atlanta, Georgia, USA

DSCC2018-9217

A DISTRIBUTED-PARAMETER CONTROL SYSTEM USING ELECTROMAGNETIC IMAGES STIMULATION FOR HUMAN-MACHINE PERCEPTION INTERFACE

Min Li[1]* **Kok-Meng Lee[1,2]***

[1] George W. Woodruff Sch. of Mech. Eng., Georgia Inst. of Tech., Atlanta, GA 30332, USA

[2] State Key Lab. of Dig. Manuf. Equip. and Tech., Sch. of Mech. Sci. and Eng.; Huazhong Univ. of Sci. and Tech., Wuhan, Hubei, China

* Corresponding Authors' Email: limin@gatech.edu, kokmeng.lee@me.gatech.edu

ABSTRACT

This article develops a new human-machine perception interface method to convert visual patterns to accurate eddy-current stimulation using an electromagnet (EM) array. The eddy-current stimulation is formulated as a feedforward controller design. In this paper, a state-space model for the eddy-current stimulation is derived for design and analysis of the controller. Unlike traditional methods where the distributed parameter systems are often modeled using partial differential equations and solved numerically using numerical methods such as finite element analysis, the model presented here offers closed-form solutions in state-space representation. The novel approach enables the applications of the well-established control theory for analyzing the system controllability. The feasibility and accuracy of the feedforward control method are numerically illustrated and validated by generating the stimulation with two types of patterns, which provides an essential base for future research of human-machine perception interface.

INTRODUCTION

The neural interface between the brain and electronics or machines are attracting more and more researchers' attention with the increasing demands of human-machine interactions [1-4]. This interface performs as a translator which converts between the electrochemical signals/language used by neutrons in the nervous system and the digital signals/language of information technology. This work has the potential to not only help deepen scientists' understanding of neural organ's underlying biology, complexity and function, but also eventually lead to new treatments for people living with movement and sensory deficits.

In perspective of the direction of the information flow, the applications of brain-machine interface can be divided into two categories: 1) Electronics/machines acquire/record neural signal from brain (in terms of bioelectricity or biomagnetism) [1,5,6]; 2) Electronics/machines transmit computer-generated signals to brain [7,8]. The former category can 'read' human mind by acquiring brain signals and control machines whereas the latter makes human 'sense' the information provided by implanted or external devices. Meanwhile, considering the mechanism of the information exchange between brain and machine, the applications can also be classified into two groups. The first group records neutrons bioelectrical activities or stimulates neutrons electrically by implanting electrical devices to human brain invasively [1,9]. Although the invasive implantation will ensure high quality of information transmission, the devices, especially for those implanted into human body, should be compact, bio-compatible and reliable. Meanwhile, the surgery for the device implantation is painful and probably leads to inflammation and other complications. Any update or malfunction of the device will result in re-implanting devices. Thereby, applications of the second group with noninvasive transmission utilizing electromagnetic field as media are also developed [7,10,12]. One good application is Transcranial Magnetic Stimulation (TMS) [13-15], which activates or suppresses regions of the nervous system (such as human brain) through exposure to the time-varying magnetic fields generated by EMs or EM arrays. This method can provide not only an approach to analyze the interaction mechanism of electrical currents with the neural systems, but also a diagnosis and treatment of psychiatric disorders, movement and sensory deficits.

An extension of TMS method is to replace the eye prosthesis which electrically stimulates the retinal neurons by implanting microelectrode arrays invasively [16-18]. By placing EM arrays above the eye to generate time-varying magnetic fields, the retinal neurons can be stimulated noninvasively [19,20]. The schematics in Fig. 1 illustrates the conceptual design of the retinal stimulator to assist the visually

impaired person interpret surroundings. With the images of surroundings captured by the camera integrated into glasses, the system extracts concise information and transmits to human by exciting an EM array placed above human eyes to stimulate the retinal noninvasively.

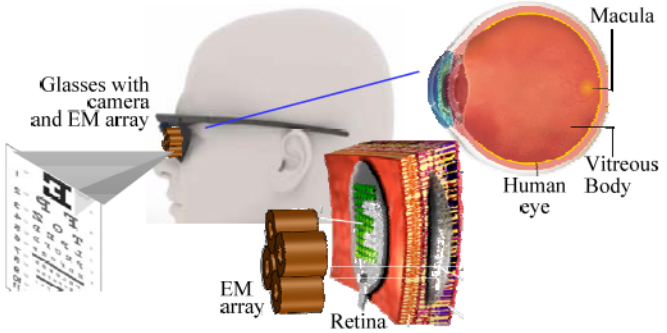

FIGURE 1 CONCEPTUAL DESIGN OF RETINA STIMULATOR

Although noninvasive transmission can avoid the disadvantages of contact transmission mentioned above, the transmission quality is relatively low and it is difficult to ensure the source and target of the transmission. The method for accurate noninvasive transmission has not been successfully achieved yet. Especially for the application of noninvasive retinal stimulation, a method to generate accurate stimulation of a certain pattern interpreting surroundings is urgently desired. The existing method can only stimulate the retinal neutron point by point (eddy-current scanning) to transmit images. Although the location of the stimulation point can be precisely controlled, the focality of eddy current is not good, and it is not time-efficient to scan the whole retinal just for one image [20]. Meanwhile, most researchers analyze the noninvasive transmission based on numerical methods, such as finite element method (FEM), which limits the application scope and calculation efficiency.

Motivated by the emerging applications of neural human-machine perception (such as prosthetic eyes) and the existing barriers mentioned above, this paper introduces a distributed-parameter control system using electromagnetic images stimulation for human-machine perception interface. The remainder of this paper is as follows.

1) The problem of the electromagnetic images stimulation is formulated as a feedforward controller design. A state-space model for the eddy-current stimulation is derived for design and analysis.
2) With the state-space model, the transfer function of the system plant consisting of an EM array and conductor is derived and the controllability of this system is analyzed by determining the row rank of the controllability matrix.
3) Based on the pre-knowledge (closed-form solutions) of the plant, the feedforward controller is designed and represented with transfer function. The feasibility and accuracy of the control method are numerically illustrated and validated by generating the stimulation with two types of patterns.

EDDY-CURRENT STIMULATION USING EM ARRAY

The schematics in Fig. 2 illustrates an eddy-current stimulation system, which can be abstracted and manifested as a typical forward control system containing a forward controller and system plant. The plant consists of an EM array with N_C EMs and a non-ferrous conductive plate. Given an ideal eddy-current pattern represented using ideal eddy current density (ECD) $\hat{\mathbf{J}}$, which is extracted from a picture, the controller estimates the excitation current $\mathbf{I}_E$ for the EM array to generate the eddy current inside the conductor. By placing the EM array at the center of the place with the EM axis perpendicular to the conductor surface, the boundary effects of the conductor will be simply ignored and the distribution of the eddy current will be purely determined by the controller. The design of forward controller is based on the previous knowledge of the plant and consists of two steps: 1) determine the needed electromagnetic energy for a desired eddy-current stimulation. 2) estimate the current input of the EM array to supply the needed electromagnetic energy.

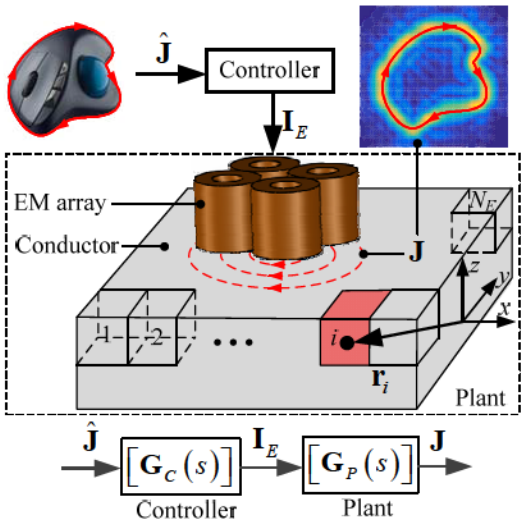

FIGURE 2 SCHEMATICS OF THE STIMULATION SYSTEM

Theoretical Modelling of Eddy Current

Assume the conductor is evenly discretized into N_E elements with their locations denoted by the displacement vector $\mathbf{r}_i$ where i=1, …, N_E, as shown in Fig. 2. Referring to Ohm's law and Maxwell's equations , the governing equation of an induced ECD $\mathbf{J}_i$ in the i^{th} element with volume v_i, the electrical conductivity $\boldsymbol{\sigma}_i = diag\left(\sigma_{ix}, \sigma_{iy}, \sigma_{iz}\right)$ and permittivity $\boldsymbol{\varepsilon}_i = diag\left(\varepsilon_{ix}, \varepsilon_{iy}, \varepsilon_{iz}\right)$ can be expressed in terms of vector potentials due to an external excitation and its neighboring elements in (1), where $\mathbf{A}_{si}$ and $\mathbf{A}_{ki}$ are the magnetic vector potentials generated by the external source and neighboring k^{th} element respective at the i^{th} element, i, k = 1, …, N_E.

$$\mathbf{J}_i = \boldsymbol{\sigma}_i \mathbf{E}_i, \text{ where } \mathbf{E}_i = -\frac{\partial}{\partial t}\left(\mathbf{A}_{si} + \sum_{k=1}^{N_E} \mathbf{A}_{ki}\right) \quad (1)$$

$\mathbf{A}_{ki} = \boldsymbol{\eta}_{\mathrm{A1}}(r_{ik})\,\mathbf{j}_k + \boldsymbol{\eta}_{\mathrm{A2}}(r_{ik})\,\mathbf{j}_k$ referring to (A.6) in Appendix A, $\mathbf{j}_i = \mathbf{J}_i \upsilon_i$ is the current source in the i^{th} element. $\boldsymbol{\eta}_{\mathrm{A1}}$ and $\boldsymbol{\eta}_{\mathrm{A2}}$ are the kernel functions of the vector potential, r_{ik} is the distance between the centers of the i^{th} and k^{th} element.

$\boldsymbol{\eta}_{\mathrm{A1}}(r_{ik}) = diag\left(\mu_{ix}, \mu_{iy}, \mu_{iz}\right)/4\pi r_{ik}$,

$\boldsymbol{\eta}_{\mathrm{A2}}(r_{ik}) = diag\left(\mu_{ix}\varepsilon_{ix}/\sigma_{ix}, \mu_{iy}\varepsilon_{iy}/\sigma_{iy}, \mu_{iz}\varepsilon_{iz}/\sigma_{iz}\right)/4\pi r_{ik}$.

Simplify (1) by representing $\mathbf{A}_{ki}$ using $\mathbf{j}_k$, $\boldsymbol{\eta}_{\mathrm{A1}}$ and $\boldsymbol{\eta}_{\mathrm{A2}}$ and assemble all N_E elements,

$$-[\mathbf{P}]\mathbf{J} = \boldsymbol{\phi} + [\boldsymbol{\eta}_{A2}]\dot{\mathbf{J}} + \left([\boldsymbol{\eta}_{A1}] + [\dot{\boldsymbol{\eta}}_{A2}]\right)\mathbf{J} + [\dot{\boldsymbol{\eta}}_{A1}]\mathbf{J} \tag{2}$$

where $\mathbf{J}\left(\in \mathbb{R}^{3N_E\times 1}\right) = \left[\mathbf{j}_1 \cdots \quad \mathbf{j}_i \quad \cdots \mathbf{j}_{N_E}\right]^{\mathrm{T}}$, $\boldsymbol{\phi} = \dot{\mathbf{A}}_s$

$\mathbf{A}_s\left(\in \mathbb{R}^{3N_E\times 1}\right) = \left[\mathbf{A}_s(\mathbf{r}_1) \quad \mathbf{A}_s(\mathbf{r}_2) \quad \cdots \quad \mathbf{A}_s(\mathbf{r}_{N_E})\right]^{\mathrm{T}}$

$[\mathbf{P}]\left(\in \mathbb{R}^{3N_E\times 3N_E}\right) = diag\left(\mathbf{P}_1, \cdots, \mathbf{P}_i, \cdots, \mathbf{P}_{N_E}\right)$;

$\mathbf{P}_i\left(\in \mathbb{R}^{3\times 3}\right) = diag\left(1/\sigma_{ix}\upsilon_i,\ 1/\sigma_{iy}\upsilon_i, 1/\sigma_{iz}\upsilon_i\right)$;

$$[\boldsymbol{\eta}_{A\ell}] = \begin{bmatrix} \boldsymbol{\eta}_{A\ell}(r_{11}) & \boldsymbol{\eta}_{A\ell}(r_{12}) & \cdots & \boldsymbol{\eta}_{A\ell}(r_{1N_E}) \\ \boldsymbol{\eta}_{A\ell}(r_{21}) & \boldsymbol{\eta}_{A\ell}(r_{22}) & \cdots & \boldsymbol{\eta}_{A\ell}(r_{2N_E}) \\ \vdots & \vdots & \boldsymbol{\eta}_{A\ell}(r_{ii}) & \vdots \\ \boldsymbol{\eta}_{A\ell}(r_{N_E1}) & \boldsymbol{\eta}_{A\ell}(r_{N_E2}) & \cdots & \boldsymbol{\eta}_{A\ell}(r_{N_EN_E}) \end{bmatrix},$$

$\ell = 1, 2.$

$\dot{\mathbf{A}}_s$ accounts for the external excitation that may be a time-varying magnetic field or relative motion between the conductor and the field; $[\dot{\boldsymbol{\eta}}_{A\ell}]$ characterizes the corresponding motion that may be due to the deflection of the conductor element and [**P**] accounts the non-uniform distribution of the electrical conductivity and element volume.

Control of Excitation Current

Given the desired eddy-current distribution **J**, the needed electromagnetic energy or input $\boldsymbol{\phi}$ in (2) is provided by the EM array. $\boldsymbol{\phi}_k$, the contribution of the k^{th} EM with the excitation current I_{Ek}, is represented using (3).

$$\boldsymbol{\phi}_k = \mathbf{A}_{sk}\dot{I}_{Ek} \tag{3}$$

where $\mathbf{A}_{sk}\left(\in \mathbb{R}^{3N_E\times 1}\right)$ represents the vector potential at all N_E elements generated by the k^{th} EM with unit excitation current. Apply (3) for all N_C EMs and assemble the equations in matrix form:

$$\boldsymbol{\phi} = \sum_{k=1}^{N_C}\boldsymbol{\phi}_k = [\mathbf{Q}]\dot{\mathbf{I}}_E \tag{4}$$

where $[\mathbf{Q}]\left(\in \mathbb{R}^{3N_E\times N_C}\right) = \left[\mathbf{A}_{s1} \quad \mathbf{A}_{s2} \cdots \quad \mathbf{A}_{sk} \cdots \quad \mathbf{A}_{sN_C}\right]$

$\mathbf{I}_E = \left[I_{E1} \quad I_{E2} \cdots \quad I_{Ek} \cdots \quad I_{EN_C}\right]^{\mathrm{T}}$.

Controllability Analysis

This stimulation system is a typical multi-input and multi-output control system, where the excitation current $\mathbf{I}_E$ and the eddy current distribution **J** are the input and output respectively. By substituting (4) into (2) and rewriting the equation, the ECD field can be estimated using state-space representation.

$$\dot{\tilde{\mathbf{J}}} = [\boldsymbol{\alpha}]\tilde{\mathbf{J}} + [\boldsymbol{\beta}]\dot{\mathbf{I}}_E \tag{5}$$

where $\tilde{\mathbf{J}} = \left[\mathbf{J} \quad \dot{\mathbf{J}}\right]^{\mathrm{T}}$, $[\boldsymbol{\beta}] = -\left[[\mathbf{0}] \quad [\boldsymbol{\gamma}]\right]^{\mathrm{T}}$, $[\boldsymbol{\gamma}] = [\boldsymbol{\eta}_{A2}]^{-1}[\mathbf{Q}]$,

$$[\boldsymbol{\alpha}] = \begin{bmatrix} [\mathbf{0}] & [\mathbf{I}] \\ -[\boldsymbol{\eta}_{A2}]^{-1}\left([\mathbf{P}] + [\dot{\boldsymbol{\eta}}_{A1}]\right) & -[\boldsymbol{\eta}_{A2}]^{-1}\left([\boldsymbol{\eta}_{A1}] + [\dot{\boldsymbol{\eta}}_{A2}]\right) \end{bmatrix}.$$

As a continuous linear time-invariant system represented in (5), the system controllability can be analyzed by determining the row rank of the controllability matrix given by

$$\begin{aligned}[\mathbf{R}] &= \left[[\boldsymbol{\beta}] \quad [\boldsymbol{\alpha}][\boldsymbol{\beta}] \quad [\boldsymbol{\alpha}]^2[\boldsymbol{\beta}] \quad \cdots \quad [\boldsymbol{\alpha}]^{6N_E-1}[\boldsymbol{\beta}]\right] \\ &= [\mathbf{M}][\mathbf{N}] = \left[\hat{\mathbf{M}}\right]\left[\hat{\mathbf{N}}\right]\end{aligned} \tag{6}$$

where $[\mathbf{M}]\left(\in \mathbb{R}^{6N_E\times 36N_E^2}\right) = \left[[\mathbf{I}] \quad [\boldsymbol{\alpha}] \quad [\boldsymbol{\alpha}]^2 \quad \cdots \quad [\boldsymbol{\alpha}]^{6N_E-1}\right]$

$[\mathbf{N}]\left(\in \mathbb{R}^{36N_E^2\times 6N_EN_C}\right) = diag\left(\underbrace{[\boldsymbol{\beta}], [\boldsymbol{\beta}], \cdots, [\boldsymbol{\beta}]}_{6N_E}\right)$,

$\left[\hat{\mathbf{M}}\right]\left(\in \mathbb{R}^{6N_E\times 18N_E^2}\right) = \left[\left[\hat{\mathbf{I}}\right] \quad [\boldsymbol{\lambda}] \quad \cdots \quad [\boldsymbol{\lambda}]^{6N_E-1}\right]$,

$\left[\hat{\mathbf{N}}\right]\left(\in \mathbb{R}^{18N_E^2\times 6N_EN_C}\right) = diag\left(\underbrace{[\boldsymbol{\gamma}], [\boldsymbol{\gamma}], \cdots, [\boldsymbol{\gamma}]}_{6N_E}\right)$

$\left[\hat{\mathbf{I}}\right]$ and $[\boldsymbol{\lambda}]^{\ell}$ are constructed by the right $3N_E$ columns of [**I**] and $[\boldsymbol{\alpha}]^{\ell}$, $\ell = 1, 2, \cdots, 6N_E - 1$; With the structure of the matrices, the rank of $\left[\hat{\mathbf{M}}\right]$ and $\left[\hat{\mathbf{N}}\right]$ are calculated as below:

$\mathrm{rank}\left(\left[\hat{\mathbf{M}}\right]\right) = 6N_E$, $\mathrm{rank}\left(\left[\hat{\mathbf{N}}\right]\right) = 6N_E \cdot \min\left(3N_E, \mathrm{rank}\left([\mathbf{Q}]\right)\right)$.

From Sylvester's inequality, the rank of [**R**] satisfies the following two inequations:

$$\mathrm{rank}\left([\mathbf{R}]\right) \le \min\left(\mathrm{rank}\left(\left[\hat{\mathbf{M}}\right]\right), \mathrm{rank}\left(\left[\hat{\mathbf{N}}\right]\right)\right) = 6N_E$$

$$\begin{aligned}\mathrm{rank}\left([\mathbf{R}]\right) &\ge \mathrm{rank}\left(\left[\hat{\mathbf{M}}\right]\right) + \mathrm{rank}\left(\left[\hat{\mathbf{N}}\right]\right) - 18N_E^2 \\ &= 6N_E\left(1 + \min\left(3N_E, \mathrm{rank}\left([\mathbf{Q}]\right)\right) - 3N_E\right)\end{aligned}$$

The system is controllable if rank([**R**]) = $6N_E$, which can be satisfied only if rank([**Q**]) = $3N_E$. The necessary condition for the controllability is $N_C \ge 3N_E$. For some applications, such as retinal stimulation, extreme accuracy of stimulation control is desired, but not seriously required. Thereby, even if there are no enough EMs, the stimulation patterns may still be acceptable by human for surrounding interpretation.

Controller Design

With the assumption of zero initial condition, the transfer function of the plant $\mathbf{G}_P(s)$ is derived by doing Laplace Transform of (2) and (4).

$$\left[\mathbf{G}_P(s)\right] = -\left[\mathbf{K}(s)\right]^{-1}[\mathbf{Q}]s \tag{7}$$

where $\left[\mathbf{K}(s)\right] = [\boldsymbol{\eta}_{A2}]s^2 + \left([\boldsymbol{\eta}_{A1}] + [\dot{\boldsymbol{\eta}}_{A2}]\right)s + \left([\mathbf{P}] + [\dot{\boldsymbol{\eta}}_{A1}]\right)$

By substituting (4) into (2), the time derivative of excitation current for the EM array $\dot{\mathbf{I}}_E$ is mathematically expressed using (8) with the assumption that $3N_E > N_C$, and rank($[\mathbf{Q}]$) = N_C.

$$\dot{\mathbf{I}}_E = -\left([\mathbf{Q}]^{\mathrm{T}}[\mathbf{Q}]\right)^{-1}[\mathbf{Q}]^{\mathrm{T}} \cdot \left([\boldsymbol{\eta}_{A2}]\ddot{\mathbf{J}} + \left([\boldsymbol{\eta}_{A1}] + [\dot{\boldsymbol{\eta}}_{A2}]\right)\dot{\mathbf{J}} + \left([\dot{\boldsymbol{\eta}}_{A1}] + [\mathbf{P}]\right)\mathbf{J}\right) \tag{8}$$

By replacing ECD $\mathbf{J}$ with ideal ECD $\hat{\mathbf{J}}$ in (8), the forward-loop controller is derived after Laplace transform.

$$\left[\mathbf{G}_C(s)\right] = -\left([\mathbf{Q}]^{\mathrm{T}}[\mathbf{Q}]\right)^{-1}[\mathbf{Q}]^{\mathrm{T}}\left[\mathbf{K}(s)\right]/s \tag{9}$$

Ideally, the output $\mathbf{J}$ would be identical to $\hat{\mathbf{J}}$, which make the overall transfer function $[\mathbf{G}_T(s)]$ to be an identity matrix. However, with the transfer functions of the controller and plant expressed in (7) and (9), the actual overall transfer function $[\mathbf{G}_T(s)]$ is derived, which is not an identity matrix.

$$\left[\mathbf{G}_T(s)\right] = \left[\mathbf{G}_P(s)\right]\left[\mathbf{G}_C(s)\right] = \left[\mathbf{K}(s)\right]^{-1}[\mathbf{Q}]\left([\mathbf{Q}]^{\mathrm{T}}[\mathbf{Q}]\right)^{-1}[\mathbf{Q}]^{\mathrm{T}}\left[\mathbf{K}(s)\right] \tag{10}$$

Thereby, even with the controller designed using (9), an arbitrary eddy-current stimulation is not guaranteed by controlling the excitation current. The desired eddy current should satisfy certain physical laws, such as charge conservation and continuity. Meanwhile, the limited number of EMs (or pseudoinverse $([\mathbf{Q}]^{\mathrm{T}}[\mathbf{Q}])^{-1}$) will make the results an optimized fit in the least-squares sense.

NUMERICAL INVESTIGATION AND DISCUSSION

Assume the electromagnetic system operates in magneto quasi-static (MQS) conditions: $2\pi L_o f \ll 1/\sqrt{\mu\varepsilon} \approx 3\times10^8$ where ε and μ are the permittivity and magnetic permeability of the conductor; f is the operating frequency, and L_o is the characteristic length of the system. The kernel functions η_{A2} in (A.6) can be ignored. The conductor is assumed isotropic, free of deformation and no relative motion between the conductor and EM array (no time derivative terms). Thereby, the transfer function of the controller can be simplified as below:

$$\left[\mathbf{G}_C(s)\right] = -\left([\mathbf{Q}]^{\mathrm{T}}[\mathbf{Q}]\right)^{-1}[\mathbf{Q}]^{\mathrm{T}}\left([\boldsymbol{\eta}_{A1}]s + [\mathbf{P}]\right)/s \tag{11}$$

With the assumption mentioned above, the eddy-current stimulation system has been numerically investigated in this section. An EM array with 5×5 EMs illustrated in Fig. 3 is placed above a conductive plate (size: 90×90×1, unit: mm) made of aluminum with the EM axis perpendicular to the plate. The details are represented in Table I. I_o and N represent the amplitude of the excitation current and number of turns respectively. The top surface of the plate is located at z_C = 5.5mm. The conductor is evenly divided into small elements with the size 1.5×1.5×1, unit: mm.

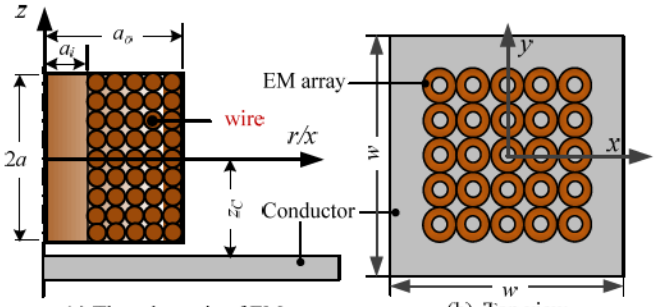

(a) The schematic of EM (b) Top view

FIGURE 3 SCHEMATICS OF EM ARRAY

Table I. Parameters of the EM

a_i	3.75mm	I_o	1A
a_o	6.5mm	N	60 #
a	2mm	z_C	5.5mm

Considering the eddy-current properties, assume the desired pattern of the eddy-current stimulation is a closed loop and the current flowing in the loop is sinusoidal with frequency f = 1kHz. Each point on the loop has the same current density without phase shift. The matrix rank of the pre-calculated $[\mathbf{Q}]$ with the given conditions is equal to the number of EM. Two types of patterns have been analyzed: 1) patterns with regular shapes, 2) patterns extracted from images.

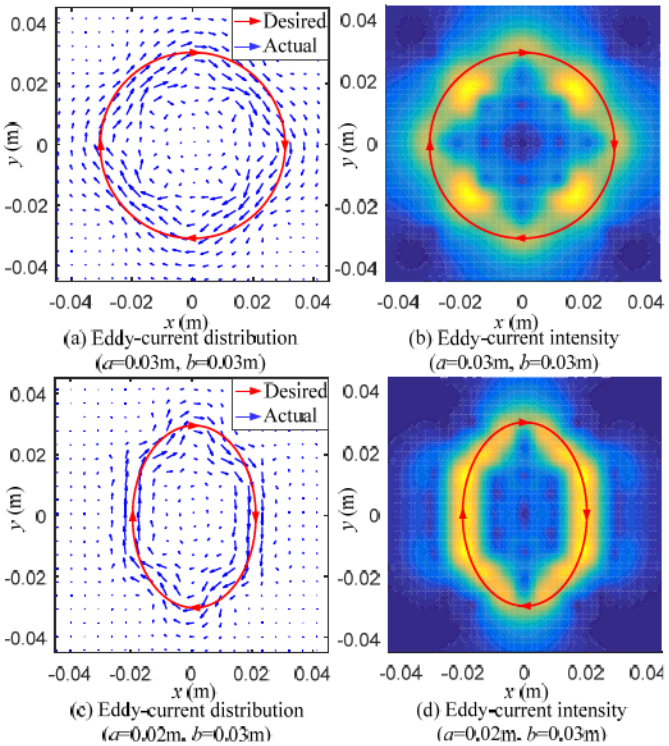

(a) Eddy-current distribution (a=0.03m, b=0.03m)
(b) Eddy-current intensity (a=0.03m, b=0.03m)
(c) Eddy-current distribution (a=0.02m, b=0.03m)
(d) Eddy-current intensity (a=0.02m, b=0.03m)

FIGURE 4 STIMULATION FOR ELLIPSE PATTERNS

Patterns with Regular Shape

Assume the desired patterns of the eddy-current stimulation have regular shapes, such as ellipses and rectangles with the centers located at the origin of the local coordinate.

Ellipse patterns have the function of $(x/a)^2+(y/b)^2=1$, where a and b are the half length of the principal axes. Four corners of the rectangular patterns are located at $(\pm c,\ \pm d)$. Given the desired stimulation patterns (ellipses and rectangles) represented using red curves with arrows in Figs. 4 and 5 and system parameters, the controller is designed using (11) and the current inputs for the EM array are estimated. Figs. 4 and 5 manifest the eddy-current stimulation for the ellipse and rectangular patterns with the estimated current inputs.

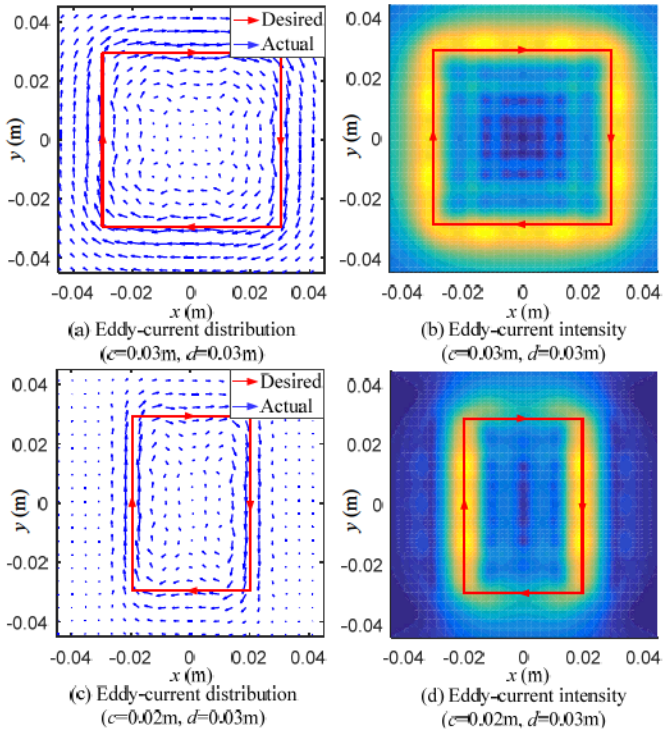

(a) Eddy-current distribution (c=0.03m, d=0.03m)
(b) Eddy-current intensity (c=0.03m, d=0.03m)
(c) Eddy-current distribution (c=0.02m, d=0.03m)
(d) Eddy-current intensity (c=0.02m, d=0.03m)

FIGURE 5 STIMULATION FOR RECTANGULAR PATTERNS

Patterns Extracted from Images

For certain applications, such as retinal stimulation, the desired patterns need to represent object contours extracted from images, which may not have regular shapes. As shown in Figs. 6 (a) and (b), the contours of a computer mouse and tree are extracted as the ideal eddy-current patterns represented by red curves. Using the same methods for the regular shape cases, the current inputs of the EM array are estimated. To analyze the effect of the EM array, a new EM array consisting of 10×10 EMs is utilized. The inside and outside diameters of the new EM are half of the original EM, which make the old and new EM array cover the same area. The matrix rank of the pre-calculated **[Q]** with the new conditions is equal to the number of EM. Figs. 6 and 7 show the distribution of the eddy current and its intensity for the old and new EM array respectively.

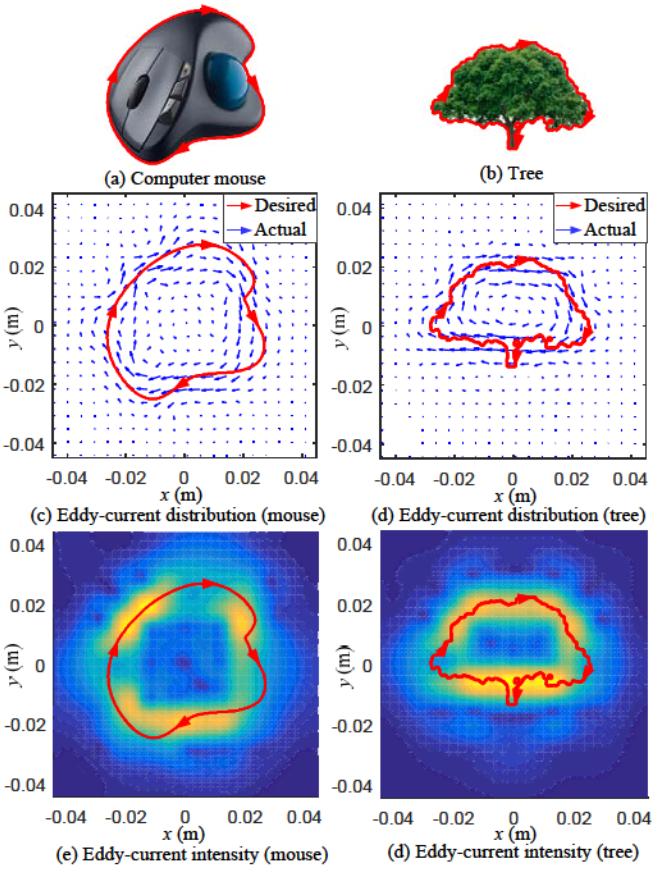

(a) Computer mouse
(b) Tree
(c) Eddy-current distribution (mouse)
(d) Eddy-current distribution (tree)
(e) Eddy-current intensity (mouse)
(d) Eddy-current intensity (tree)

FIGURE 6 STIMULATION FOR IMAGE PATTERNS (25 EMS)

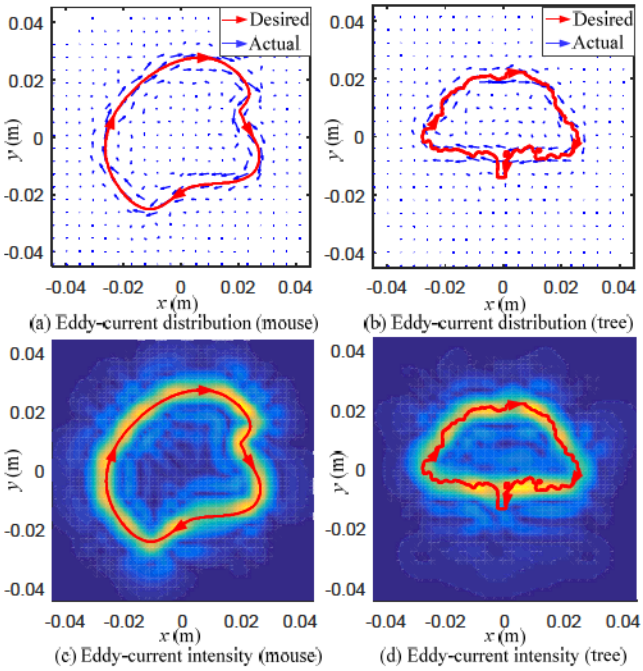

(a) Eddy-current distribution (mouse)
(b) Eddy-current distribution (tree)
(c) Eddy-current intensity (mouse)
(d) Eddy-current intensity (tree)

FIGURE 7 STIMULATION FOR IMAGE PATTERNS (100 EMS)

Results Analysis and Discussion

Some observations can be made from the simulation results from Fig. 4 to Fig. 7.

- The 5×5 EM array can successfully generate eddy-current stimulation similar to the given regular shape patterns and the patterns extracted from images.
- Instead of being a single current loop represented by the red curve, the generated eddy-current stimulation covers all the target and generates high intensity of eddy current at desired locations.
- The simulation results of the regular shape cases are better than those of the image cases due to the limited number and regular layout of EMs.
- By increasing the density of EM in the EM array (10×10 EMs), more accurate eddy-current stimulations are generated as illustrated in Fig. 7.

CONCLUSION

This article has developed a new human-machine perception interface method to convert visual patterns to accurate eddy-current stimulation using an electromagnet (EM) array. By discretizing the conductor, the state-spacing model for eddy-current stimulation is derived for design and analysis. The transfer function of the system plant consisting of an EM array and conductor is obtained and the controllability of this system is analyzed by determining the row rank of the controllability matrix. Based on the pre-knowledge (closed-form solutions) of the plant, the feedforward controller is designed and represented with transfer function. Numerical investigation has demonstrated that this method can successfully generate eddy-current stimulation given regular and irregular patterns at desired locations and the accuracy of the stimulated patterns increases with the increase of the EM number.

ACKNOWLEDGMENTS

This work was supported in part by the U. S. National Science Foundation EFRI-M3C-1137172, CMMI-1662700, National Science Foundation of China under Grant U1713204, and National Basic Research Program of China (973 Program, Grant No. 2013CB035803).

REFERENCES

[1] Hochberg, L. R., Serruya, M. D., Friehs, G. M., Mukand, J. A., Saleh, M., Caplan, A. H, and Donoghue, J. P., "Neuronal ensemble control of prosthetic devices by a human with tetraplegia," *Nature*, Vol. 442, No. 7099 (2006): pp. 164–171.

[2] Velliste, M., Perel, S., Spalding, M. C., Whitford, A. S., & Schwartz, A. B., "Cortical control of a prosthetic arm for self-feeding," *Nature*, Vol. 453, No. 7198 (2008): pp. 1098–1101.

[3] Hochberg, L. R., Bacher, D., Jarosiewicz, B., Masse, N. Y., Simeral, J. D., Vogel, J., Haddadin, S., et al. "Reach and grasp by people with tetraplegia using a neurally controlled robotic arm." *Nature,* Vol. 485, No. 7398 (2012): pp. 372-375.

[4] Stavisky, S. D., Kao, J. C., Nuyujukian, P., Ryu, S. I., and Shenoy, K. V., "A high performing brain–machine interface driven by low-frequency local field potentials alone and together with spikes." *Journal of neural engineering*, Vol. 12, No. 3 (2015): pp. 036009.

[5] Ando, H., Takizawa, K., Yoshida, T., Matsushita, K., Hirata, M., and Suzuki, T., "Wireless multichannel neural recording with a 128-Mbps UWB transmitter for an implantable brain-machine interfaces." *IEEE Trans. on biomedical circuits and systems*, Vol. 10, No. 6 (2016): pp. 1068-1078.

[6] Liu, X., Zhang, M., Xiong, T., Richardson, A. G., Lucas, T. H., Chin, P. S, Ralph Etienne-Cummings, Tran, T. D., and Van der Spiegel, J., "A Fully Integrated Wireless Compressed Sensing Neural Signal Acquisition System for Chronic Recording and Brain Machine Interface." *IEEE Trans. on biomedical circuits and systems*, Vol. 10, No. 4 (2016): pp. 874-883.

[7] Cao, X., Cai, D., Zhang, X., Liu, R., and Tang, J., "Optimization of Electric Field Distribution of Multichannel Transcranial Magnetic Stimulation Based on Genetic Algorithm." *Processing of the IEEE Biomedical Engineering and Informatics (BMEI), 2010 3rd International Conference on*, pp. 1544-1547, Yantai, China, Oct. 16-18, 2010.

[8] Yang, S., Xu, G., Wang, L., Geng, Y., Yu, H., and Yang, Q., "Circular Coil Array Model for Transcranial Magnetic Stimulation," *IEEE Trans. on Applied Superconductivity*, Vol. 20, No. 3 (2010): pp. 829–833.

[9] Simeral, J. D., Kim, S. P., Black, M. J., Donoghue, J. P., and Hochberg, L. R., "Neural control of cursor trajectory and click by a human with tetraplegia 1000 days after implant of an intracortical microelectrode array." *Journal of neural engineering*, Vol. 8, No. 2 (2011): pp. 025027.

[10] McFarland, D. J., Sarnacki, W. A., and Wolpaw, J. R., "Electroencephalographic (EEG) control of three-dimensional movement." *Journal of neural engineering*, Vol. 7, No. 3 (2010): pp. 036007.

[11] McFarland, D. J., Krusienski, D. J., Sarnacki, W. A., and Wolpaw, J. R. "Emulation of computer mouse control with a noninvasive brain–computer interface." *Journal of neural engineering*, Vol. 5, No. 2 (2008): pp. 101.

[12] Schalk , G., Miller, K. J., Anderson, N. R., Wilson, J. A., Smyth, M. D., Ojemann, J. G., Moran, D. W., Wolpaw, J. R., and Leuthardt, E. C.. "Two-dimensional movement control using electrocorticographic signals in humans." *Journal of neural engineering*, Vol. 5, No. 1 (2008): pp. 75.

[13] Tzabazis, A., Aparici, C. M., Rowbotham, M. C., Schneider, M., Etkin, A., and Yeomans, D. C., "Shaped Magnetic Field Pulses by Multicoil Repetitive Transcranial Magnetic Stimulation (rTMS) Differentially Modulate Anterior Cingulate Cortex Responses and Pain in

Volunteers and Fibromyalgia Patients." *Molecular Pain*, Vol. 9, No. 33 (2013): pp. 1–9.

[14] Avenanti, A., Coccia, M., Ladavas, E., Provinciali, L. and Ceravolo, M. G., "Low-frequency rTMS Promotes Use-dependent Motor Plasticity in Chronic Stroke." *Neurology*, Vol. 78, No. 4 (2012): pp. 256–264.

[15] Rubi-Fessen, I., Hartmann, A., Huber, W., Fimm, B., Rommel, T., Thiel, A., and Heiss, W. D., "Add-on Effects of rTMS on Subacute Aphasia Therapy: Enhanced Improvement of Functional Communication and Basic Linguistic Skills. A Randomized Controlled Study." *Archives of physical medicine and rehabilitation*, Vol. 96, No. 11 (2015): pp. 1935-1944.

[16] Margalit, E., Maia, M., Weiland, J. D., Greenberg, R. J., Fujii, G.. Y., Torres, G.., Piyathaisere, D. V., O'Hearn, T. M., Liu, W. T., Lazzi, G.., Dagnelie, G.., Scribner, D. A., Juan. Jr, E. D. and Humayun, M. S., "Retinal Prosthesis for the Blind." *Survey of Ophthalmology*, Vol. 47, No. 4 (2002): pp. 335-356.

[17] Humayun, M. S., de Juan, E., Dagnelie, G., Greenberg, R. J., Propst, R. H., and Phillips, D. H., "Visual Perception Elicited by Electrical Stimulation of the Retina in Blind Humans." *Arch Ophthalmic*, vol. 114, No. 1 (1996): pp. 40-46.

[18] Bonmassar, G.., Lee, S. W., Freeman, D. K., Polasek, M., Fried, S. I. and Gale, J. T., "Microscopic Magnetic Stimulation of Neural Tissue." *Nature Communications*, Vol. 3 (2012): pp. 921–931.

[19] Shin, J. Y., Ahn, J. H., Pi, K., Cho, D. I. D., and Goo, Y. S. (2015, November), "Electrodeless, Non-invasive Stimulation of Retinal Neurons Using Time-varying Magnetic Fields." *Proceeding of the IEEE Sensors*: pp. 1-4, Busan, South Korea, Nov. 1-4, 2015.

[20] Lee, K. -M., Lin, C. Y., and Li, M., "A Continuous-Field Actuation Method for Transducing Optical Color Images to Magnetic/Eddy-Current Patterns." *Proceeding of the ASME 2015 Dynamic Systems and Control Conference*: pp. V003T45A006, Columbus, Ohio, Oct. 28-30, 2015.

[21] Lim, J. Y., and Lee, K. -M., "Distributed Multi-Level Current Models for Design Analysis of Electromagnetic Actuators," *IEEE/ASME Trans. Mechatronics*, Vol. 20, No. 5 (2015): pp. 2413-2424.

APPENDIX A

Electromagnetic Model with Displacement Current

Assume a non-magnetic conductor is placed in the space filled with time-varying magnetic field and there is no external current inside the conductor. Applying Maxwell' equation inside the conductor domain:

$$\nabla \times \frac{1}{\mu}\mathbf{B} = \mathbf{J} + \frac{\partial \mathbf{D}}{\partial t} \qquad \text{(A. 1)}$$

where $\mathbf{B}$ is the magnetic flux density (MFD), $\mathbf{J}$ is the ECD inside the conductor, $\mathbf{D}$ is the displacement field with the expression $\mathbf{D} = \varepsilon \mathbf{E}$, μ and ε are the permeability and permittivity of the conductor respectively.

MFD can be represented by the magnetic vector potential $\mathbf{A}$ using (A.2):

$$\mathbf{B} = \nabla \times \mathbf{A} \qquad \text{(A. 2)}$$

Substituting (A.2) into (A.1) with $\mathbf{D} = \varepsilon \mathbf{E}$ and Ohm's law ($\mathbf{J} = \sigma \mathbf{E}$),

$$\nabla \times \left(\frac{1}{\mu} \nabla \times \mathbf{A} \right) = \mathbf{J}_P, \text{ where } \mathbf{J}_P = \mathbf{J} + \frac{\varepsilon}{\sigma} \dot{\mathbf{J}} \qquad \text{(A. 3)}$$

Here, $\mathbf{J}_P$ is named equivalent current density. With the condition of $\nabla \bullet \mathbf{A} = 0$, (A.3) can be simplified as below,

$$\nabla^2 \mathbf{A} = -\mu \mathbf{J}_P \qquad \text{(A. 4)}$$

The magnetic vector potential $\mathbf{A}(\mathbf{r})$ at location $\mathbf{r}$ generated by the current $\mathbf{J}_P$ in the small volume V' can be calculated by solving (A.5).

$$\mathbf{A}(\mathbf{r}) = \frac{\mu}{4\pi} \int_{V'} \frac{\mathbf{J}_P(\mathbf{r}')}{|\mathbf{r} - \mathbf{r}'|} dv' \qquad \text{(A. 5)}$$

With the assumption that the dimension of the volume is relatively much smaller than the distance between $\mathbf{r}$ and the volume, $\mathbf{A}(\mathbf{r})$ can be approximately expressed with (A.6) [21].

$$\mathbf{A}(\mathbf{r}) \approx \frac{\mu}{4\pi R} \mathbf{J}_P V' = V' \left[\eta_{A1}(R) \mathbf{J} + \eta_{A2}(R) \dot{\mathbf{J}} \right] \qquad \text{(A. 6)}$$

where $\eta_{A1}(R) = \frac{\mu}{4\pi R}, \eta_{A2}(R) = \frac{\mu\varepsilon}{4\pi R\sigma}$, $R = |\mathbf{r} - \overline{\mathbf{r}}|$,

$\mathbf{e} = \frac{1}{R}(\mathbf{r} - \overline{\mathbf{r}})$, $\overline{\mathbf{r}}$ is the location of the center of the volume.